Barkhordarian, A.; Storch, H.v.; Zorita, E.; Loikith, P.C.; Mechoso, C.R.:
Observed warming over northern South America has an anthropogenic origin
In: Climate Dynamics (2017) Springer

DOI: 10.1007/s00382-017-3988-z

Observed warming over northern South America has an anthropogenic origin

Armineh Barkhordarian[1,2], Hans von Storch[3], Eduardo Zorita[3], Paul C. Loikith[4], Carlos R. Mechoso[1,2]

[1]*Department of Atmospheric and Oceanic Sciences. University of California, Los Angeles (UCLA)*

[2]*Jet Propulsion Laboratory, California Institute of Technology. Pasadena, California, USA*

[3]*Institute of Coastal Research, Helmholtz-Zentrum Geesthacht, Geesthacht, Germany*

[4]*Portland State University, Department of Geography, Portland Oregon, USA*

We investigate whether the recently observed trends in daily maximum and minimum near-surface air temperature (Tmax and Tmin, respectively) over South America (SA) are consistent with the simulated response of Tmin and Tmax to anthropogenic forcing. Results indicate that the recently observed warming in the dry seasons is well beyond the range of natural (internal) variability. In the wet season the natural modes of variability explain a substantial portion of Tmin and Tmax variability. We demonstrate that the large-scale component of greenhouse gas (GHG) forcing is detectable in dry-seasonal warming. However, none of the global and regional climate change projections reproduce the observed warming of up to 0.6 K/Decade in Tmax in 1983-2012 over northern SA during the austral spring (SON). Thus, besides the global manifestation of GHG forcing, other external drivers have an imprint. Using aerosols-only forcing simulations, our results provide evidence that anthropogenic aerosols also have a detectable influence in SON and that the indirect effect of aerosols on cloud's lifetime is more compatible with the observed record. In addition, there is an increasing trend in the observed incoming solar radiation over northern SA in SON, which is larger than expected from natural (internal) variability alone. We further show that in the dry seasons the spread of projected trends based on the RCP4.5 scenario derived from 30 CMIP5 models encompasses the observed area-averaged trends in Tmin and Tmax. This may imply that the observed excessive warming in the dry seasons serve as an illustration of plausible future expected change in the region.

1. Introduction

There is increased interest in understanding anthropogenic global warming in specific regions. The Amazonian region includes about one half of the world's tropical forests and is a key component of the global carbon cycle (Cox et al., 2000). Exbrayat and Williams (2015) suggest that biomass loss due to deforestation in the Amazon alone has contributed approximately 1.5% to the increase in atmospheric CO2 concentrations over the last decade. In addition to the greenhouse gas forcing, land-use changes due to expanding agricultural activities and black carbon aerosols from biomass burning are potentially the most important external drivers of climate change over South America (SA) (Exbrayat and Williams, 2015). Smoke aerosols released from biomass burning in the Amazon and Savannah regions, as well as pollution emitted from mega cities have very large effects on the net energy input to the atmosphere (Procopio et al., 2004, Lin et al, 2006). Natural phenomena are also associated with climate change and variability over SA including the effects of atmosphere/ocean modes of climate variability. According to the Working Group I contribution to the Fifth Assessment Report (AR5) of the Intergovernmental Panel on Climate Change (IPCC 2013), near-surface temperature over SA has been increasing over the last several decades. Consistently, the retreat of tropical glaciers has accelerated, especially since the late 1970s (area loss between 20 and 50%; Bradley et al., 2009). The AR5 report states with medium confidence that over SA warm extremes are increasing in severity and frequency while cold extremes are decreasing (IPCC 2013). The observed temperature trends from the beginning of the observational record to 2010 averaged over SA are consistent with the simulated response to combined natural and anthropogenic forcings by the CMIP5 (Coupled Model Intercomparison Project 5) models (Knutson et al. (2013); De Barros Soares et al. (2016)).

In this study, we employ global and regional climate models to determine whether the SA climate has changed as a result of global increases in greenhouse gas concentrations. Being able to distinguish the externally driven changes in observed trends from those that are internally generated will help to understand the present-day climate and motivate actions to cope with the consequences of future climate change. With this goal, we will assess in the first step whether the observed changes are likely to have been due to natural (internal) variability alone, and if not, whether they are consistent with the simulated response to anthropogenic forcing.

Moreover, we examine for the first time to what extent the observed climate trends in SA are already an indication of the conditions described by the climate change scenarios at the end of this century. The approach we use has been earlier applied to the climate variables over the Mediterranean and Baltic Sea region (Barkhordarian et al. 2012b, 2013, 2016). In the present study, we focus on changes in daily minimum/maximum temperature (Timn and Tmax, respectively) and incoming solar radiation over SA. By linking past changes to expected future changes, this research will contribute to provide an illustrative example of what a future climate influenced by enhanced greenhouse gas concentration might look like. Our finding will inform policy makers about plausible climate changes through scientific analysis by distinguishing between natural and anthropogenic causes, which is critical to assessing the impact of mitigation plans and developing adaptation strategies.

The remainder of this paper is structured as follows. Details on the observational and model data are given in Sect. 2. The methodology used in this study is discussed in Sect.3. The results including the detection, influence of modes of natural climate variability and the attribution, are shown in Sect. 4. Surface solar radiation analysis is shown in Sect. 4.3. The dependence on the period selected to calculate trends is discussed in Sect. 4.4. The main conclusions and discussions are presented in Sect.5.

2. Observations and model data

The observed temperature record is from the latest version of the Climate Research Unit's (CRU) gridded high resolution (0.5° by 0.5°) dataset CRU TS 3.24.01, which is available from 1901 to 2015 [Harris et al 2014]. In this study, we do not use CRU data before 1951 because of the scarcity of stations especially over northern South America. The station records in this dataset are quality controlled and homogenized using the automated method proposed in Easterling and Peterson [1995]. For surface solar radiation a continuous and validated climate data record (CDR) based on the Meteosat First Generation (MFG) satellites is used [Posselt et al 2011]. For the climate change projections, we consider 30 global climate simulations with coupled AOGCMs. Here we use all available models to assess the robustness of the results against the influence of model difference (Supp. Table 1 indicates the list of the models and the number of simulations). The output of these simulations is provided through the CMIP5 archive, which include projections driven by future GHG atmospheric concentrations following the Representative Concentration Pathway 4.5 (RCP

4.5, [Meinshausen et al., (2011)]). In order to capture the fine scale structure of climate change signals, we further use MPI-CSC-REMO2009 regional climate simulations driven by MPI-ESM-LR from WCRP CORDEX [Jones et al., 2011]). In addition, 10 CMIP5 model simulations are used to estimate the response to different external forcings. We further use long pre-industrial control integrations of CMIP5 climate models, which are pre-industrial control experiment with all forcing held constant.

3. Methodology

We follow the research methodology presented in Barkhordarian et al. (2012b, 2013, 2016). In the first step, we assess whether the observed changes in Tmin and Tmax are compatible with an undisturbed stationary climate and, if not, whether they are consistent with the modeled response to anthropogenic forcing. The comparison between observations and simulations is carried out using correlation statistics and regression indices (Barkhordarian et al. 2013). The response to external forcing is defined either as the simulated trends in the observational period or as the trend obtained in future climate simulations.

3.1. Anthropogenic climate change signal estimate

In this study, we use two approaches to estimate anthropogenic climate change signals (GHG and aerosols). In the first approach, we use single forcing runs for the historical period, which is available for only a subset of CMIP5 models. From the single forcing runs we consider 2 groups of simulations. One group (GHG) includes 29 simulations conducted by 7 models forced with historical well-mixed greenhouse gases only (BCC-CSM1-1, CanESM2, CNRM-CM5, CSIRO-Mk3-6-0, GISS-E2-H, GISS-E2-R, IPSL-CM5A-LR). A second group (AA) includes 10 simulations conducted by 3 models forced with anthropogenic aerosols only (CanESM2, CSIRO-Mk3-6-0, NorESM1-M). In these simulations, aerosol emissions (or concentrations) are allowed to vary in time whereas all other forcing variables are set to preindustrial values. In the multi-model ensembles mean of 7 models (29 GHG simulations), the internal variability is reduced by about 90 percent, which leads to an enhanced signal-to-noise ratio in estimated signal patterns.

For the second definition of the climate response, we use time-slice climate change experiments and define the anthropogenic climate change signal (Greenhouse gas and Sulfate aerosols, GS) as the difference between the last decades of the 21st century (2071– 2100, RCP4.5 scenario) and the

reference climatology (1961– 1990). We assume a linear development in multi-decadal running means from 1961–2100 and the resulting signal is scaled to change per year (Bhend and von Storch, 2009).

We further subdivided the AA simulations into two groups to separately investigate the impact of aerosol concentration on, (1) cloud droplet radius and cloud droplet concentration, which is known as the "first indirect effect" or "cloud albedo effect" [Ramaswamy et al., 2001], and (2) cloud lifetime, depth, and liquid water content, which is known as either the "second indirect effect" or "cloud lifetime effect" [Lohmann and Feichter, 2005]. Hence, AA1 simulations include both the first and second indirect effect, while AA2 simulations include the first indirect effect only. These simulations (GS, GHG, AA1 and AA2) will be used to identify the primary drivers of observed trends of Tmin and Tmax over SA.

4. Results

Figures 1 and 2 present a comparison of the observed spatially averaged change of the seasonal mean Tmax and Tmin, respectively over the period from 1983-2012 together with the multimodel ensemble mean response to different external forcings. The forcings considered include greenhouse gas and sulfate aerosols (GS), greenhouse gas only (GHG), and anthropogenic aerosols only, both with and without the "cloud lifetime effect" of aerosols (AA1 and AA2, respectively). Over SA, the observed record indicates an upward trend in Tmin and Tmax in all seasons, with a maximum rate of increase in SON (September-November) and minimum in MAM (March-May). Both Tmax and Tmin have their lowest levels of variability in DJF (December-February), with that of Tmax variability larger than Tmin (red whiskers in Figs 1 and 2). Regarding the spatial pattern of changes the warming is observed throughout the region. The maximum values are over central Brazil in the dry seasons (JJA, SON), although some areas of cooling are also notable along the west coast of SA in both Tmin and Tmax. A cooling of up to -0.2 K/Decade in Tmax is pronounced in DJF along the extratropical west coast of northern Chile, the Andes of Bolivia, Ecuador and southwestern Colombia. The observed cooling, we find in the observation along the extratropical west coast of SA is consistent with other studies (e.g., Falvey and Gerreaud 2009; Schulz et al., 2012; Vuille et al., 2015).

The increasing trends in Tmax and Tmin have been observed and also projected by the global and regional climate models used in this study in response to GHG forcing (Figs 1 and 2, respectively).

The CORDEX model agrees with the suite of all 30 CMIP5 models in projecting a general warming across SA with largest values over the tropical latitudes, based on RCP4.5 scenarios (See Sup. Figs 1 and 2). The agreement found between the CMIP5 and CORDEX simulations leads to the conclusion that projected warming over SA is robust against substantial modifications in the configuration of the climate models. The projected warming is more pronounced in Tmax with values up to +0.4 k/decade over central Brazil in SON. Similar features were found in the former generation of global [Blázquez et al (2012)] and regional climate change projections based on A1B (A2) scenarios [Urrutia and Vuille (2009); Nuñez et al (2009); Marengo et al (2009); Sánchez et al (2015)]. It is important to note that none of the 30 global climate simulations and the regional climate simulation used in this study reproduce the observed warming of up to +0.6 K/Decade in Tmax over Brazil and northern Argentina in SON (Sup Figure 1).

As shown in Figs 1 and 2, the observed positive trends in Tmin and Tmax contrast with the negative trends obtained in the aerosol-only AA2 simulations without the "cloud lifetime effect" of aerosols (purple bars in Figs 1 and 2). However, the AA1 simulations that consider the "cloud lifetime effect" of aerosols obtain a small positive trend in Tmin and Tmax (red bars in Figs 1 and 2). Such a difference may indicate that the direct aerosol–radiation interactions results in a net cooling. However, when the changes in clouds due to radiatively absorbing aerosol are considered, the reduction in cloud cover increases the net short-wave radiation reaching the surface, producing a warming that counteracts the direct aerosol cooling (Archer-Nicholls et al., 2016).

4.1. Detection of externally forced changes

In this section, we assess whether the observed trend of Tmin and Tmax presented above can be due to natural (internal) variability alone. To do so, seasonal observed trends are compared with the estimated natural (internal) variability derived from control integrations of CMIP5 climate models. From 20,000-simulated years of control runs we draw 600 non-overlapping 30-year segments to estimate the natural (internal) variability of 30-year trends. The observed trend is likely not due to natural (internal) variability alone if it lies outside the 2.5%-97.5% quantile range of the control runs. Therefore, externally forced changes are detectable in cases where the 97.5th percentile confidence interval (red whiskers in Figures 1 and 2, one tailed test) excludes zero. The results indicate that externally forced changes are detectable (at 2.5% level) in observed trends of

Tmax in JJA and SON (Fig 1). In terms of Tmin, externally forced changes are detectable in all seasons except MAM (Fig 2).

Regarding the spatial pattern of change, Fig. 3 (middle column) shows regions where the externally forced changes are detectable in observed trends of Tmax over 1983-2012. Similarly, Fig. 4 (middle column) shows regions where externally forced changes have a detectable influence in observed changes of Tmin (at 2.5% level). These results provide evidence that in SON and JJA the observed warming of up to 0.6 K/Decade over the central Brazil and northern Argentina in 1983-2012 is above the expected range of natural (internal) fluctuations. Some regions with cooling mostly for Tmax are also detectable over Ecuador, Colombia, the Andes of Bolivia (Figs 3 and 4, middle column) that can't be explained by natural (internal) variability.

4.1.1. Influence of modes of natural climate variability

Numerous studies have identified strong connections between the SA climate and atmospheric and oceanic modes of climate variability, namely, the El Niño Southern Oscillation (ENSO) [Marengo 1992], the Pacific Decadal Oscillation (PDO) [Mantua and Hare 2002], and the Southern Annular Mode (SAM) [Thompson and Wallace 2000]. The study by Loikith et al (2017) demonstrates that ENSO, PDO, Atlantic Niño, and SAM show significant relationships with extreme temperature months over South America. The observed significant and sustained warming during 2000-2010 over Amazonia has been found related to SST anomalies in the tropical Atlantic during the JAS season and SST anomalies in the central/east Pacific during the JFM season (Jiménez-Muñoz et al., 2013). It is now recognized that CMIP5 models tend to underestimate the amplitude of these climate modes of variability [e.g. Kumar et al., 2013, Chadwick et al., 2015]. Such an underestimation of the simulated internal climate variability may lead to a spurious detection result, if as a consequence the simulated natural internal variability is of smaller amplitude than the real one. Therefore, in this section, we explore the consequences of subtracting from the observations that part of the temperature variability that can be attributed to the natural modes of climate (ENSO, PDO and SAM). We regress the detrended temperature time series on the detrended ENSO index for each grid box separately. The slope of the regression is ENSO signal or fingerprint. This signal is removed from the observations and control simulations by subtracting the trend in the ENSO index times the ENSO signal [Bhend and von Storch, 2009, Barkhordarian et al, 2013]. The normalized climate indices are from ECA&D (European Climate Assessment and

Datasets).

As shown in Fig. 3 (left column) if the signals of these three climate modes are removed, the observed cooling trends in Tmax disappear over Ecuador, Colombia, the Andes of Bolivia, and northern Chile. The study by Falvey and Garreaud (2009) also partially attributed the observed cooling along the west coast of SA to the Pacific decadal variability. Vuille et al., (2015) also shows that the coastal cooling is consistent with the observed PDO fingerprint. Loikith et al., (2017) demonstrates that ENSO is highly influential on the occurrence of extreme temperature months over coastal northwestern SA and that over Patagonia, the SAM is highly influential during spring and fall. According to Figure 3 (right column) in the wet seasons (DJF and MAM), the trend in Tmax after removing the fingerprint of the climate modes remained distinguishable in a few grid cells, indicating that the three natural modes of variability explain a substantial portion of Tmax variability in wet seasons. However, in the dry seasons (JJA, SON) the observed warming trends over northern SA are robust against removing the signal of the three natural climate modes (Figs 3 and 4, right column). We note that natural modes of variability such as ENSO and PDO might themselves be affected by greenhouse gas and aerosols emissions. Thus, in future work we will attempt to distinguish whether the trends in natural modes are themselves forced by external forcing or whether they are the results of internal variability alone that are underestimated by GCMs.

The results obtained indicate that the warming in Tmin and Tmax for JJA and SON over the northern SA exceeds the limits of natural (internal) variability. These results are robust against the removal of the fingerprint of the ENSO, PDO and SAM. That is, externally forced changes are robustly detectable (at 2.5% level). In the following, we assess whether the observed trends, which are found to be inconsistent with natural (internal) variability, are consistent with what climate models simulate as the response of daytime (Tmax) and nighttime (Tmin) temperature to anthropogenic forcing.

4.2. Attribution of observed trends to anthropogenic forcing

Having established that externally forced changes are detectable in the observed record of Tmax and Tmin, we determine in a second step whether these results are consistent with what climate models simulated as expected response to anthropogenic forcing. This continent accounts for an estimated 15% of global fire emissions of carbon from landscape fires and open biomass burning

(van der Werf et al., 2010), with regional hotspots of fire activity around the edges of Amazonia. Therefore, in what follows we use GS, GHG, AA1 and AA2 simulations to identify the primary drivers of observed trends of Tmin and Tmax over SA. The comparison is carried out using spatial correlation statistics and regression between the trend spatial patterns (for more details, see Barkhordarian et al. [2012b]).

In SON, the correlation between the observed trend pattern and the GS (Greenhouse gas and Sulfate aerosols, GS) response pattern derived from each of the 30 GCMs (Sup. Table 1) is in the range of [0.72, 0.87], while that with the GS response pattern derived from CORDEX RCM is 0.88. The correlation with the historical GHG response pattern is 0.87. These correlations are larger than the 97.5^{th} %tile distribution of correlation coefficients between 600 patterns of unforced trends and the anthropogenic signal patterns. The correlation between the observed trend pattern and the AA1 response pattern is 0.70. However, there is a negative correlation with the AA2 response pattern. This difference in correlations indicates that the observed trends are distinct from the predicted response to aerosols in simulations that do not include the cloud-lifetime effect.

Also, in JJA the observed trend pattern shows a relatively high positive correlation with the anthropogenic signal patterns. This correlation is in the range of [0.70, 0.85] with the 30 GS response pattern, 0.80 with regional GS response pattern, and 0.81 with historical GHG response pattern. These coefficients are also larger than the 97.5^{th} %tile distribution of the correlations derived from control runs. Indeed, such correspondence can hardly be expected to accrue if the effect of anthropogenic forcing where not present in the observed record.

Figure 5 displays the seasonal regression indices and the 97.5^{th} %tile uncertainty range derived from fits of the regression model to 600 control run segments derived from 20,000-year control simulations. The quantiles of the regression indices (R) of control run segments onto the anthropogenic climate change signal patterns (GS, GHG, AA1, AA2) are used to test the H_d hypothesis that the distribution of regression indices is only due to internal variability. This hypothesis can be rejected at the prescribed level of significance if the 97.5^{th} %tile uncertainty range does not include "zero". When there is insufficient evidence to reject H_d, and the 97.5^{th} %tile uncertainty range includes "unity", the consistency of observed changes to the respective forcing is claimed (Barkhordarian et al., 2016).

As shown in Figure 5 in JJA and SON the uncertainty interval of R does not include zero, but includes unity in the case of all 30-global projected GS signals (black bars), one-regional projected GS signal (green bar) and the simulated GHG signal (blue bars). Therefore, as the regression indices within all the 30 GS and GHG signal patterns are significantly greater than zero and compatible with a value of unity, we conclude that the large-scale component of GHG (GS) signal is compatible (with less than 2.5% risk of error) with the observed positive trends of Tmax in dry seasons.

Aerosols-only forcing simulations without the "cloud lifetime effect" of aerosols (AA2) display near zero or negative regression indices in all seasons (purple bars in Fig 5). However, AA1 simulations that include the aerosol-radiation-cloud's lifetime interactions, yield regression indices significantly greater than zero in JJA and SON (red bars in Fig 5), indicating that including the second indirect effect of aerosols on cloud's lifetime yields results that are more compatible with the observed record.

4.3. Surface Solar radiation (indirect effect of aerosols)

The sum of the direct and diffuse shortwave radiation reaching the surface is denoted as Surface Solar Radiation (SSR). At decadal time-scale regional SSR changes are mostly the result of changes in atmospheric transparency due to changes in cloud and/or changes in the anthropogenic aerosols. Anthropogenic aerosols exert both a direct (clear-sky scattering of solar radiation) and indirect (impact on cloud microphysical and radiative properties) effect on climate. These effects are associated with large uncertainties in climate simulations [*Forster et al.*, 2007]. The most important factor of this uncertainty is the complex interactions between aerosols and clouds [e.g. Lohmann and Freichter, 2005]. To our knowledge, no study exists that assesses the consistency of observed SSR trends with climate change projections over SA.

The analysis of satellite SSR data indicates a positive trend in warm seasons (SON, DJF) that is in on order of +5.3 W/m^2/decade in SON over northern SA. In contrast, trends are negative in cold seasons (MAM, JJA). A strong solar dimming in the order of -6 W/m^2/decade is observed in cold seasons over southern SA. The range of changes of solar radiation solely due to natural climate variability, derived from the 20,000-year pre-industrial simulations, indicate that observed trends of SSR over SA cannot be explained by natural (internal) variability alone (at 2.5% level). Regions

where the observed trends are significantly larger than zero are shown in Figure 7 (left column). Therefore, we conclude that there are external drivers at work in the observed record of solar radiation reaching the surface.

In contrast to the large trends in the observations, climate change projections based on RCP4.5 scenario simulate very small trends in all seasons as a response of SSR to GHG forcing (Fig 7, right column). It is likely, therefore, that an additional external forcing is required to explain the discrepancy. For example, the regionally changing anthropogenic aerosol loading in the atmosphere may contribute to determine the observed SSR trends.

4.4. Dependence on the Period Selected to Calculate Trends

In this subsection, we investigate how dependent our results are on the exact time period selected for analysis. Figure 8 shows the seasonal regression indices of moving 30-year trend patterns of Tmax and Tmin based on CRU over 1952-2012 onto the ensemble mean GHG response pattern. The gray shaded area indicates the 97.5^{th} %tile distribution of regression indices, derived from control simulations, onto the ensemble mean GHG response pattern. Detection of an GHG signal can be claimed in those cases where the gray shaded area in Fig 8 excludes zero while consistency with GHG signal pattern is claimed in cases where the gray shaded area does not include zero but includes unity.

As shown in Fig. 8 (first row) for Tmax in JJA and SON, the gray-shaded area does not include the zero line but includes a regression coefficient equal to unity for 30-year trends over period ending in 2000 and later. This indicates the emergence of a compatible GHG influence in daily maximum temperature trends in dry seasons in the 21^{st} century. However, in the wet seasons (DJF, MAM) the regression indices are either negative or not significantly greater than zero. For Tmin Fig. 8 (second row) shows that the effect of GHG signal is compatible with observations in DJF, JJA and SON in 30-year trends over period ending in 1997 and later.

We further assess the seasonal regression indices of observed moving 30-year trend pattern of Tmax and Tmin, over the period 1952–2012, onto the anthropogenic aerosols (AA1) response pattern. As shown in Figure 9, for Tmax in JJA and SON, and for Tmin in SON the gray-shaded area does not include the zero line but includes unity for 30-year trends over period ending in 2008 and later. This indicates that the effect of aerosols is compatible with observations in 30-year trends

over period ending in 2008 and later. **Major sources of aerosols over Brazil are the burning of biomass [Rosário et al., 2013]. Brazil stands out in terms of biomass burning, with approximately 190,000 points of detection of fires in 2010, with most of these points occurred in the southern part of the Amazon basin during the dry season (July- November) [CPTEC/INPE (http://www.cptec.inpe.br); Mariano et al., 2014].**

5. Discussions and conclusions

In this study, we investigate whether the climate over South America has changed because of human activity since the beginning of the industrial revolution. We also examine to what extent the recently observed changes in daily minimum and daily maximum temperature are consistent with climate change AR5 projections. In the first step of our methodology, we assess whether the observed changes can be explained as due to natural (internal) variability alone, and if not, whether they are consistent with what models simulate as response to anthropogenic forcing.

Our results indicate that, over the past decades, observed warming trends in Tmin and Tmax in the dry seasons (JJA, SON) over northern SA cannot be explained by natural (internal) variability alone and that externally forced changes have an influence (at the 2.5% level) on the observed warming trends. The detection of externally forced changes in Tmin and Tmax in the dry seasons are robust against the removal of the fingerprint of the three natural modes. However, in the wet season, the natural modes of variability explain a substantial portion of Tmax and Tmin variability. The pattern correlation and regression analyses clearly capture the concerted emergence of greenhouse gas (GHG) signal in the 21st century. The detection of GHG effect is largely independent of the choice of model from which we drive the expected climate change signal. However, none of the global and regional climate change projections, used in this study, reproduce the observed warming of up to 0.6 K/Decade in Tmax over 1983-2012 over northern SA in austral spring (SON). Thus, we conclude that besides the regional manifestation of GHG forcing and assuming that the GHG response is correctly simulated, other external drivers have an imprint. This conclusion is strengthened when computing the diurnal temperature range (DTR = T_{max} minus T_{min}), which is a relevant indicator of climate change due to the asymmetry between maximum and minimum temperature response to anthropogenic forcing [Braganza et al., 2004]. Several studies highlight a significant decreasing trend in the DTR over the last 50 yr at global scale [see Vose et al., 2005 and references therein]. The large increase of minimum daily temperatures

compared to a much smaller enhancement of maximum temperatures over land is responsible of such global DTR changes. Nevertheless, over South America the CRU observed record indicates that DTR is increasing in dry seasons and decreasing in wet seasons. The increasing trend in DTR of almost +0.03 K/decade in SON and JJA over 1983-2012 indicates a faster increase in Tmax than Tmin. Climate models underestimate the observed trends in DTR because of underestimating the observed daytime warming amplification. It is notable that if an increased GHG were a significant driver of the observed warming over SA, we would expect to see nights warming faster than days. The opposite results obtained here could indicate that although GHG is the dominant driver of Tmin, other external forcing than GHG have an imprint in observed Tmax and is responsible for the daytime warming amplification over northern SA.

Using aerosols-only forcing simulations with and without the second indirect effect of aerosols, our results provide evidence that anthropogenic aerosols also have a detectable influence in SON and that the indirect effect of aerosols on cloud's lifetime is more compatible with the observed record.

We further show a positive trend in the incoming solar radiation over the northern SA in SON that cannot be explained by natural (internal) variability alone and that this trend is distinct from the expected response to GHG forcing. The study by Hodnebrog et al., (2014) demonstrates that the forcing due to the increased black carbon emissions and a shorter black carbon (BC) lifetime, leaves the direct aerosol effect of BC virtually unchanged. However, it has a side effect diminishing the fraction of low cloud cover over a zonal band from Equator to 15°S (Hodnebrog et al., 2014). Given that the emission of anthropogenic sulfate aerosols (SO_2) over SA is almost constant (See Sup. Fig. 3), and that the emissions of black carbon are increasing during the dry seasons [van der Werf et al., 2010], we suggest that the positive trend in incoming solar radiation could partly be attributed to changes in clouds due to radiatively absorbing aerosol. This effect increases the net short-wave radiation reaching the surface by reducing cloud cover, producing a daytime warming amplification and consequently increasing diurnal temperature range observed over SA in the last decades. In global scale, fossil fuel black carbon is found to have a detectable contribution to the near-surface warming over the last 50yr of the 20th century (Jones et al., 2011). We note that, there is another important driver active in this region, namely land-cover change, which is not consider in the present study.

We further show that in dry seasons the spread of projected trends based on the RCP4.5 scenario derived from 30 CMIP5 models encompasses the observed area-averaged trends in Tmin and Tmax. This may imply that the observed excessive warming in dry seasons serve as an illustration of plausible future expected change in the region.

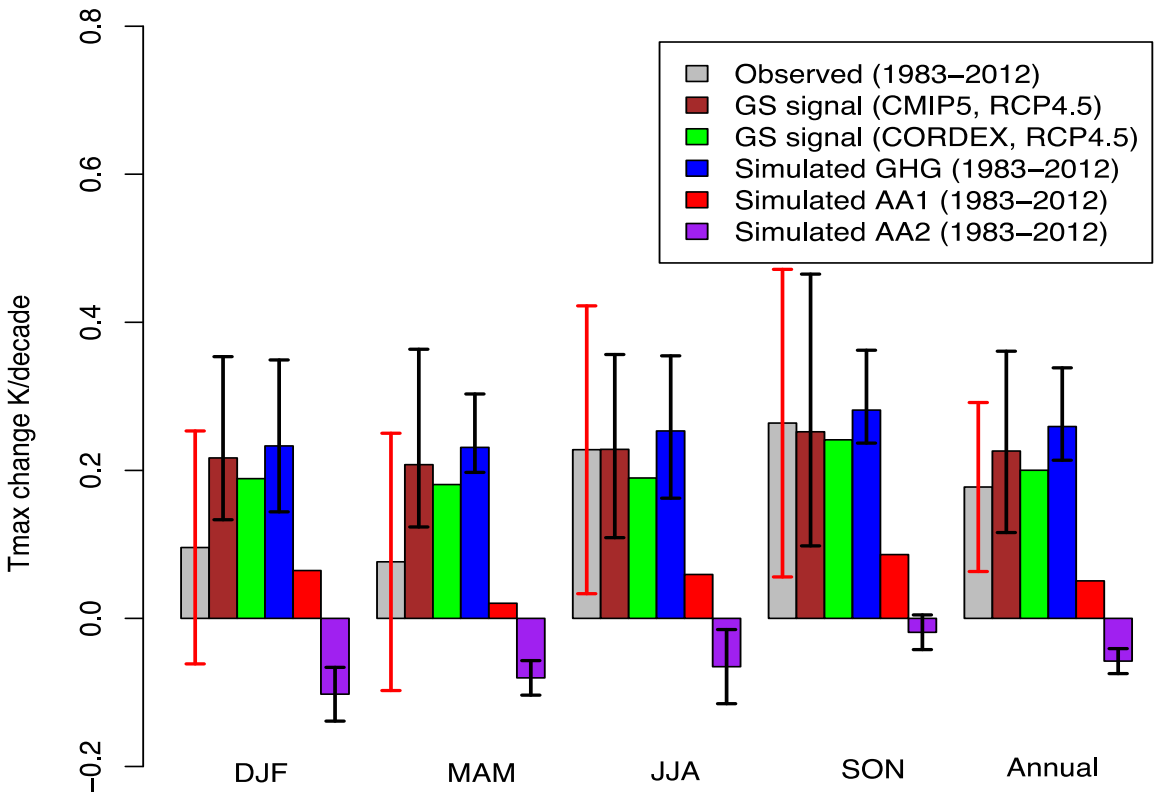

388

389 **Figure 1:** Observed area averaged changes in daily maximum temperature (Tmax) over the period
390 1983–2012 (grey bars) in comparison with 30 global climate change projections estimated from
391 time slices experiment (2071-2100 minus 1961-1990), RCP4.5 scenario (GS, brown bars), one
392 regional climate change projections (GS, green bars), the historical GHG forcing only simulations
393 over 1983-2012 (GHG, blue bars), the historical aerosols forcing only simulations with (AA1, red
394 bars), and without (AA2, purple bars) the "cloud lifetime effect" of aerosols. *The vertical axes*
395 show the area averaged change of Tmax. The black whiskers indicate the spread of trends of
396 simulations. The red whiskers indicate the 97.5th %tile uncertainty range of observed trends,
397 derived from 20,000-year control runs. Units are K per Decade.

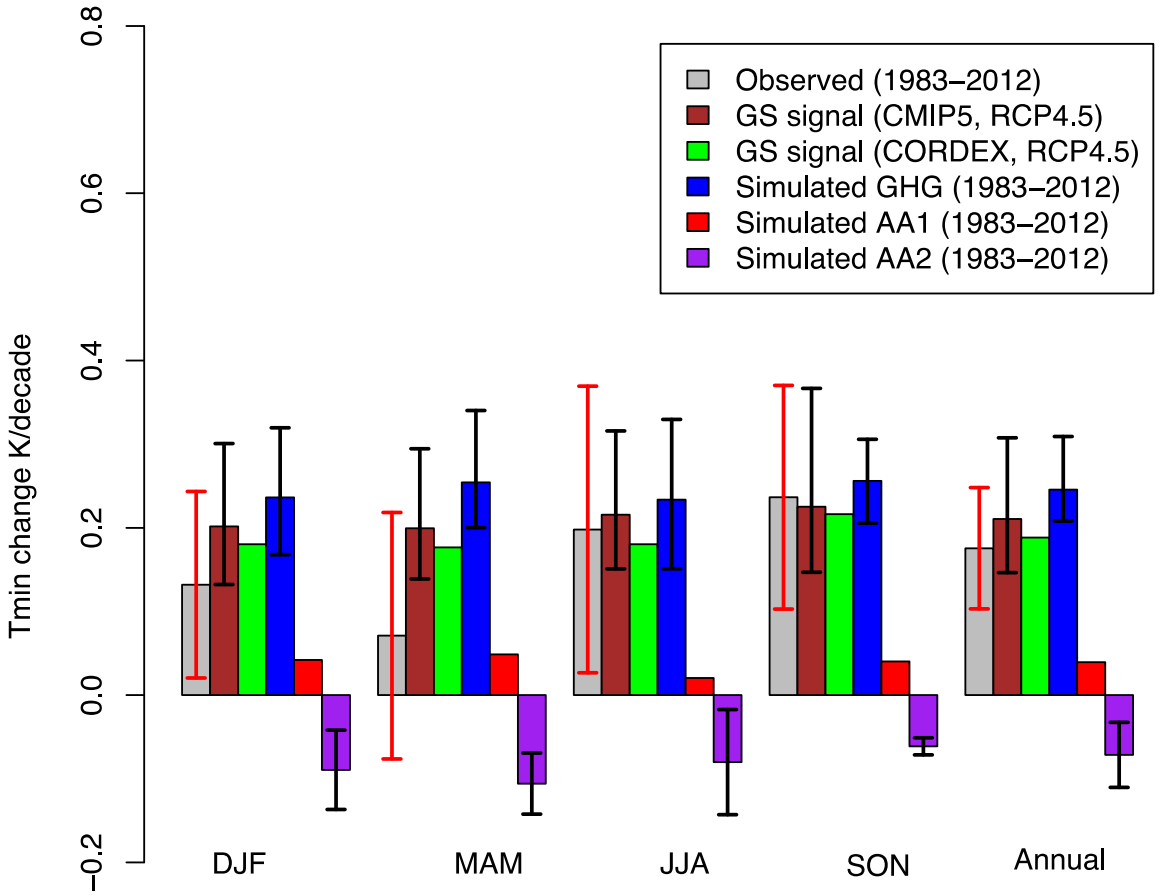

398

399 **Figure 2:** Same as Figure 1, but for daily minimum temperature (Tmin). *The vertical axes show*

400 the area averaged change of Tmin.

401

402

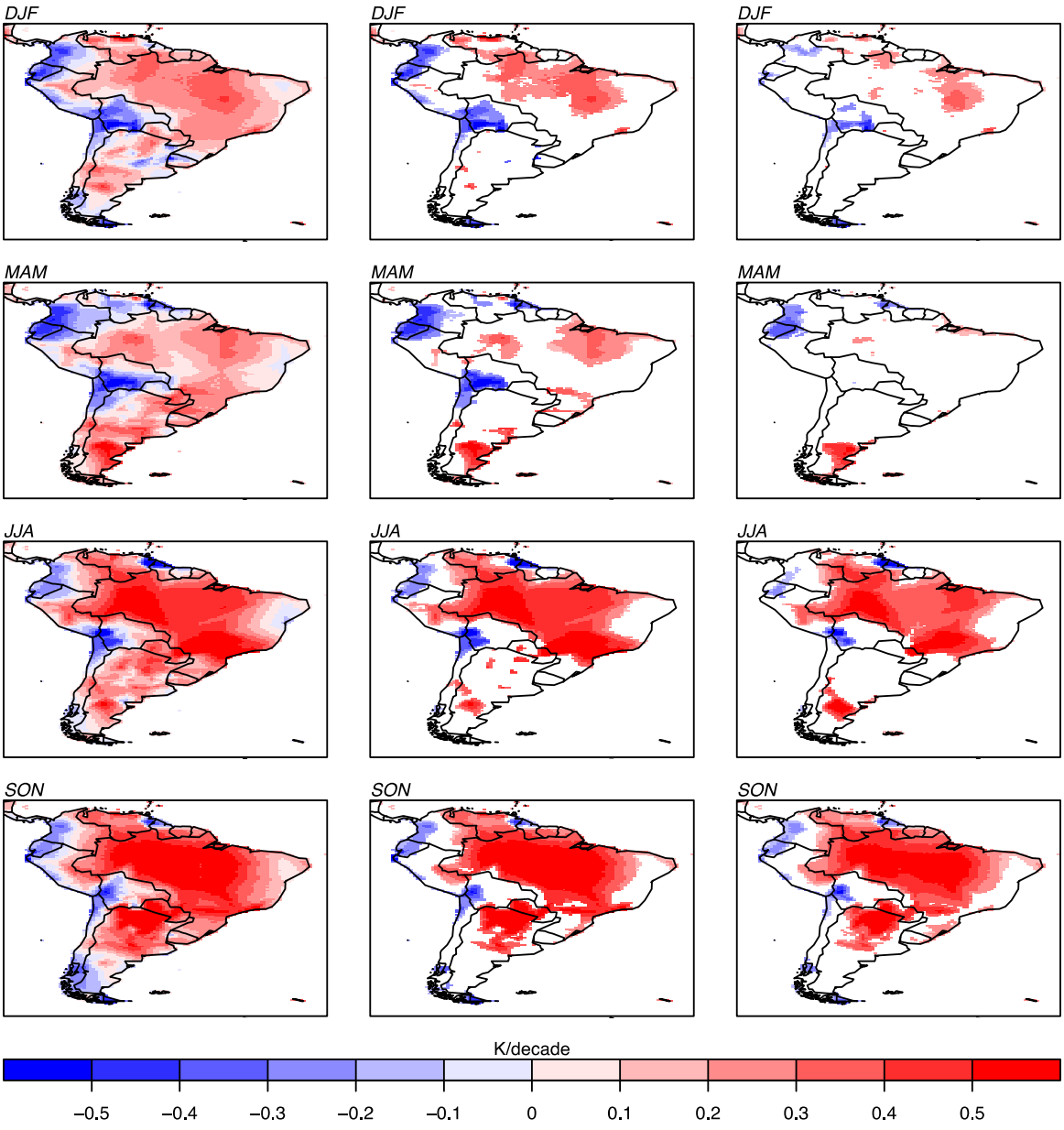

Figure 3: left column: Seasonal observed trend of daily maximum temperature (Tmax) over 1983-2012-time period based on CRU dataset. Middle column: Areas where externally forced changes are detectable (at 2.5% level) in the observed record of Tmax, based on 20,000-year control simulations. Right column: Areas where the detection of externally forced changes is robust against removing the fingerprint of three natural modes (ENSO, PDO and SAM).

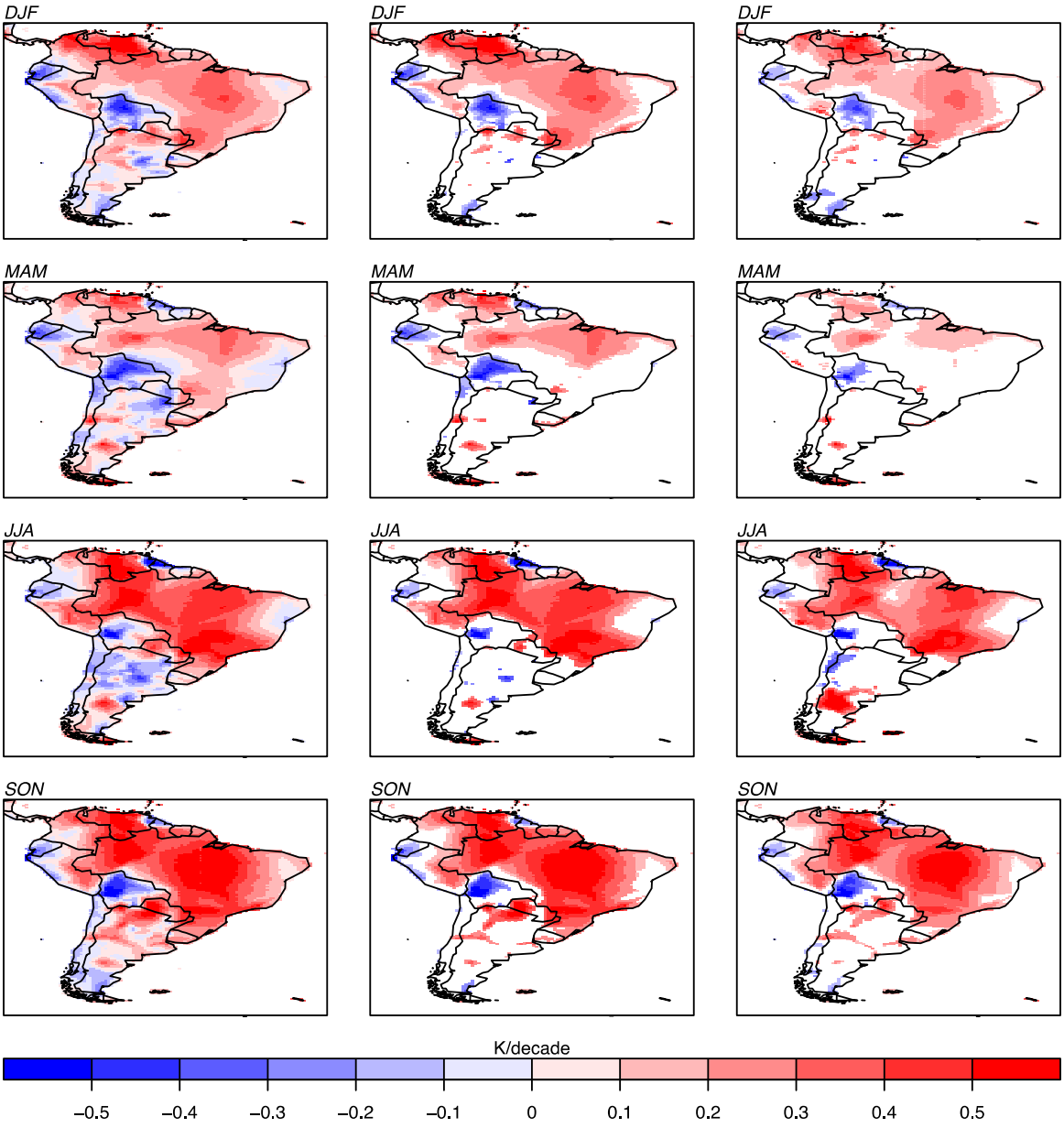

Figure 4: Same as Figure 3, but for daily minimum temperature (Tmin).

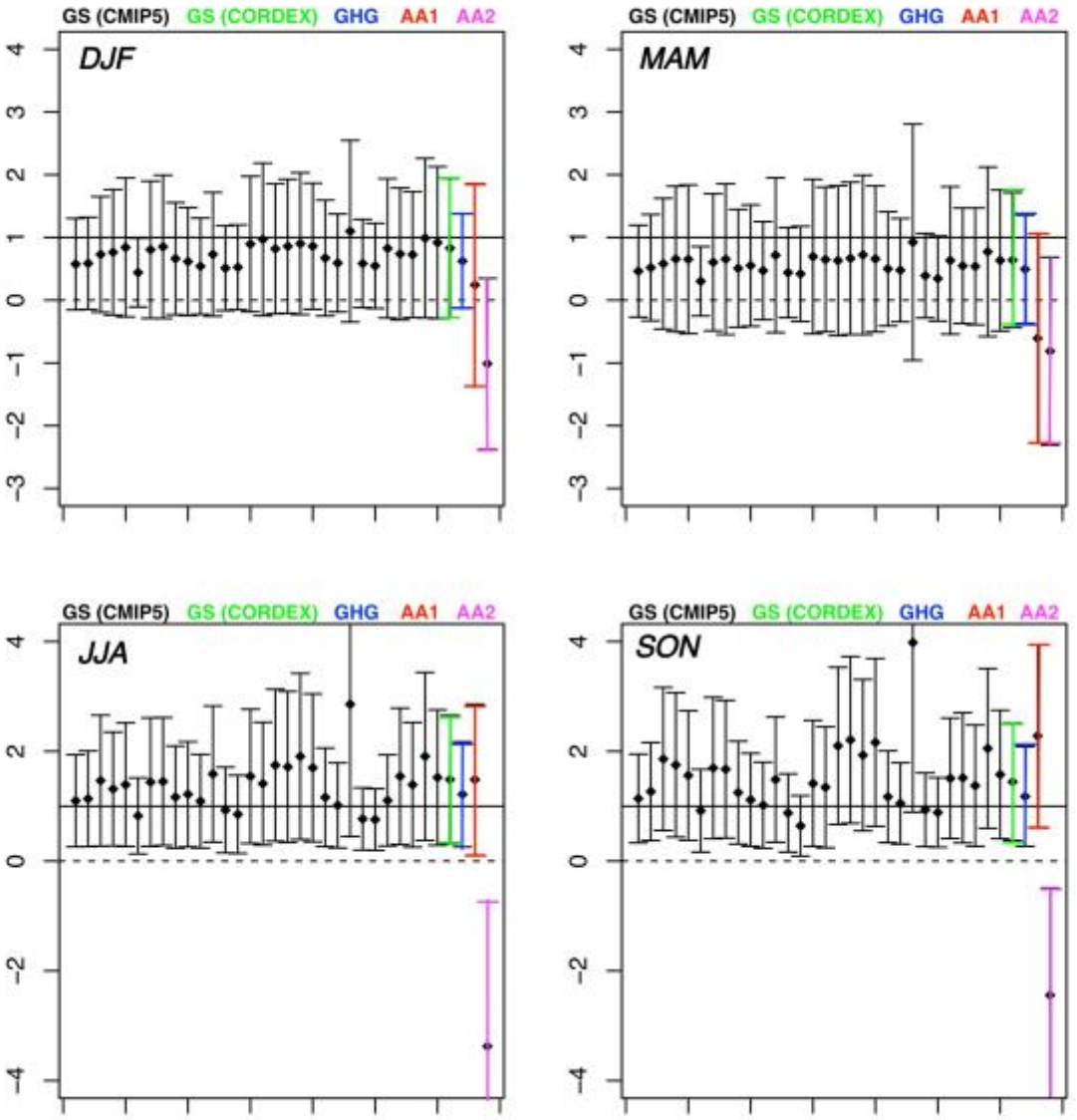

Figure 5: Seasonal regression indices of observed trend pattern of daily maximum temperature against the 30-global projected GS signal patterns (black bars), against 1 regional projected GS signal pattern (green bar) the simulated GHG signal pattern (blue bar), the simulated anthropogenic aerosols signal patterns with (red bar) and without (purple bars) the "cloud lifetime effect". The 97.5th %tile uncertainty range of regression indices is derived from 20,000-year pre-industrial control simulations from CMIP5 archive. *The vertical axes* show regression indices.

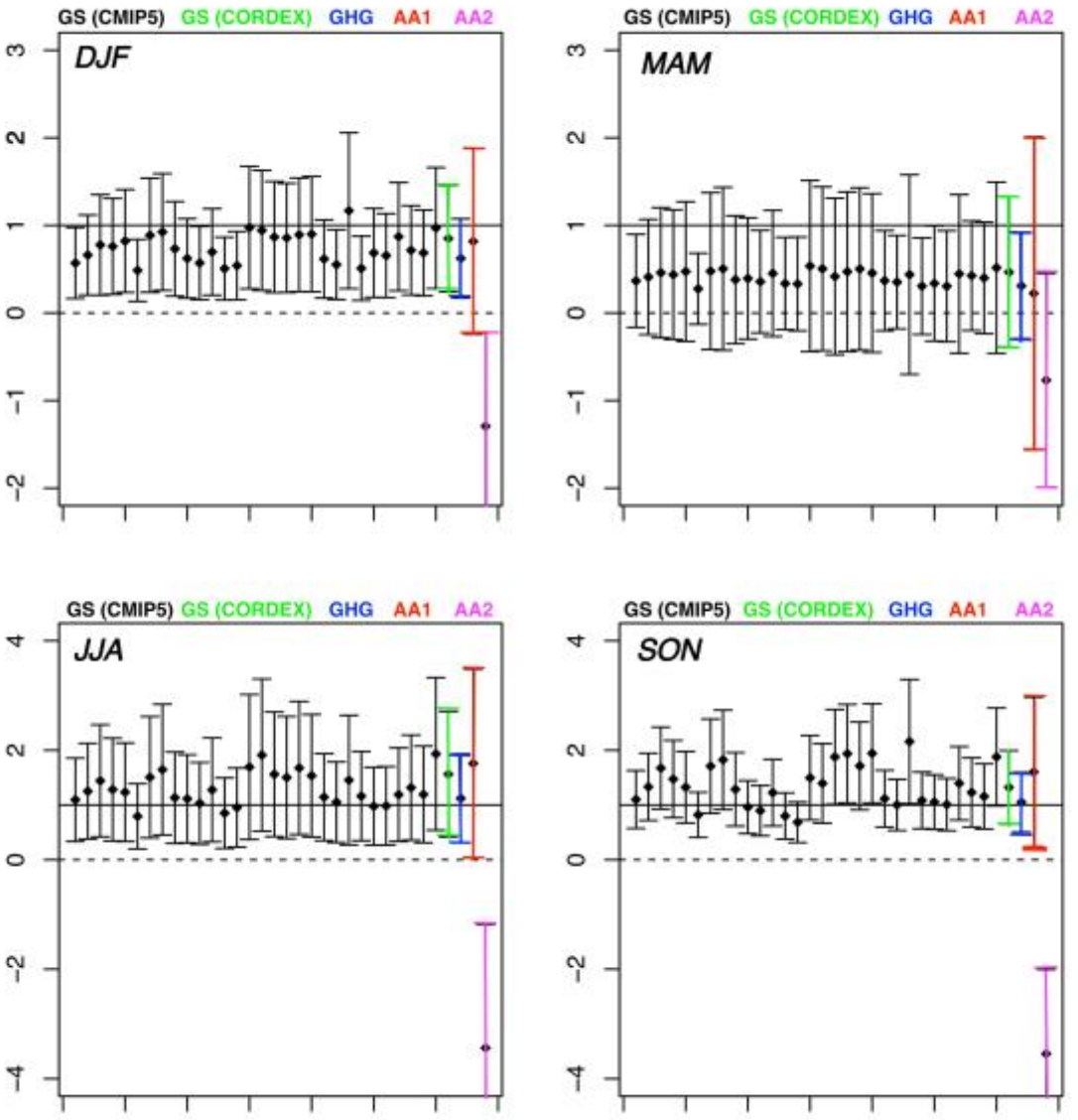

Figure 6*:* Same as Figure 5, but for daily minimum temperature (Tmin).

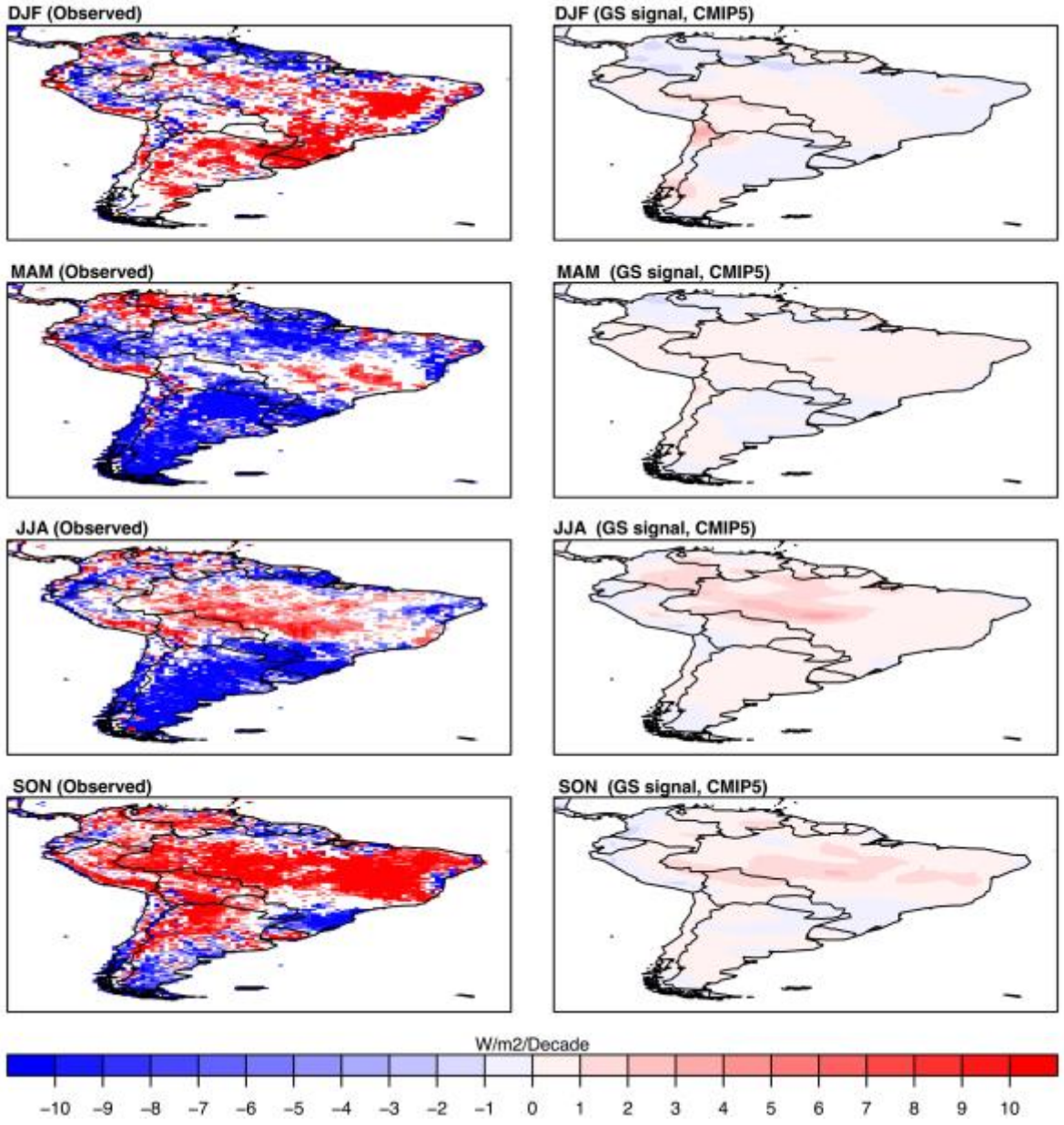

Figure 7: left column: Seasonal observed patterns of change in surface solar radiation (SSR) according to the CDR satellite data. Displayed trends are significantly greater than zero (at 2.5% level). Missing grid cells indicate regions where the observed trend lies within the range of trends solely due to natural (internal) variability, based on long control simulations. Right column: GS (Greenhouse gas and Sulfate aerosols, GS) signal pattern estimated from time slices of climate projection 2071-2100 minus 1961-1990 mean scaled to change per decade) according to the RCP4.5 scenario. Unites are W/m2/Decade.

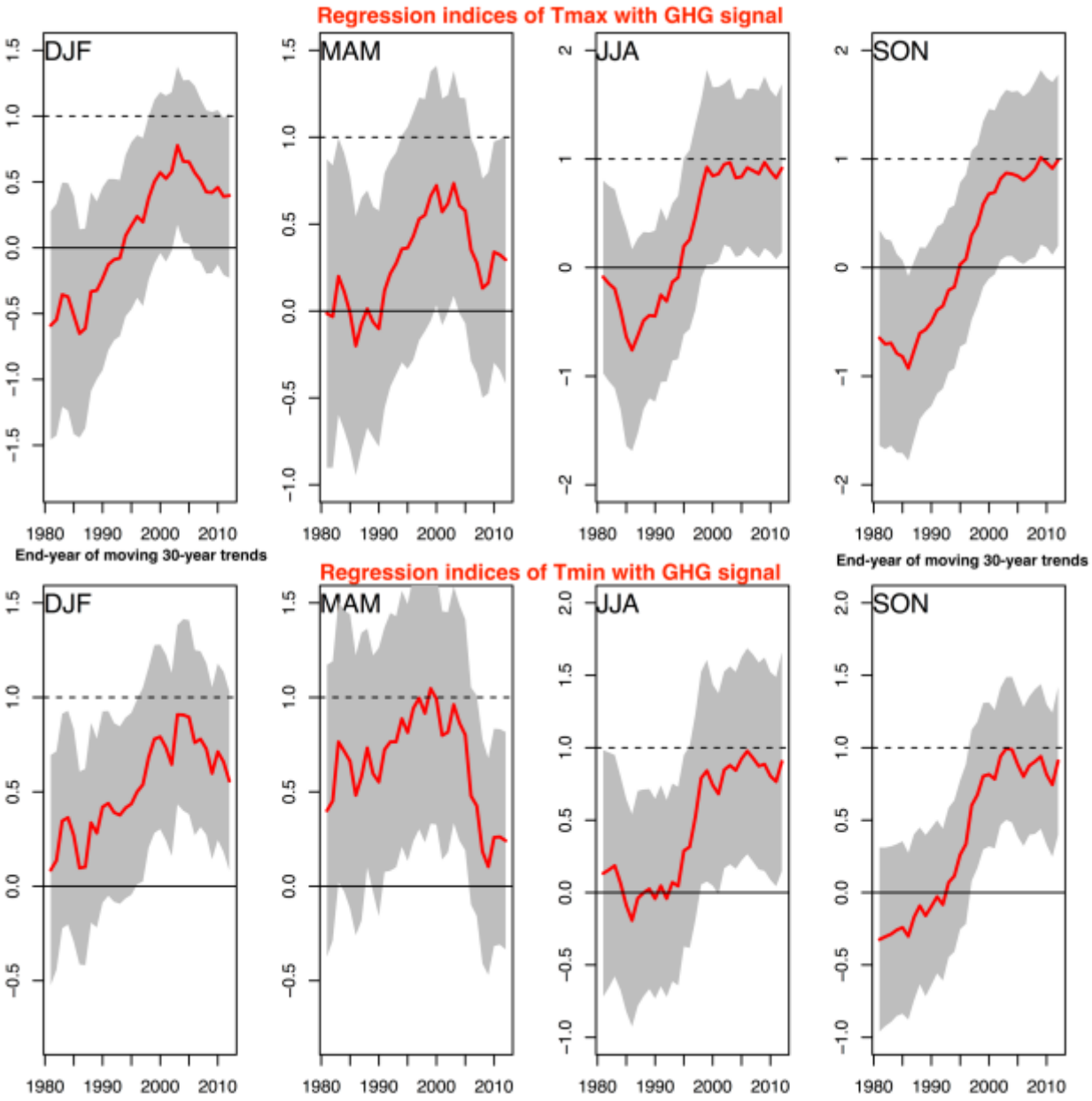

Figure 8: First (second) row seasonal regression indices of observed moving 30-year trend pattern of Tmax (Tmin), over the period 1952–2012, onto the ensemble mean GHG response pattern. *The vertical axes* denote the regression indices. *The horizontal axes* show the end-year of moving 30-year trends. The grey shaded area indicates the 97.5% range of regression indices in a stationary climate derived from 600 non- overlapping control run segments. *The dotted lines* mark regression indices equal to unity, and *the solid lines* mark regression indices equal to zero. Detection of a GHG signal can be claimed in those cases where the gray shaded area excludes "0" and consistency with GHG signal pattern is claimed in cases where the gray shaded area does not include "0" but includes "1".

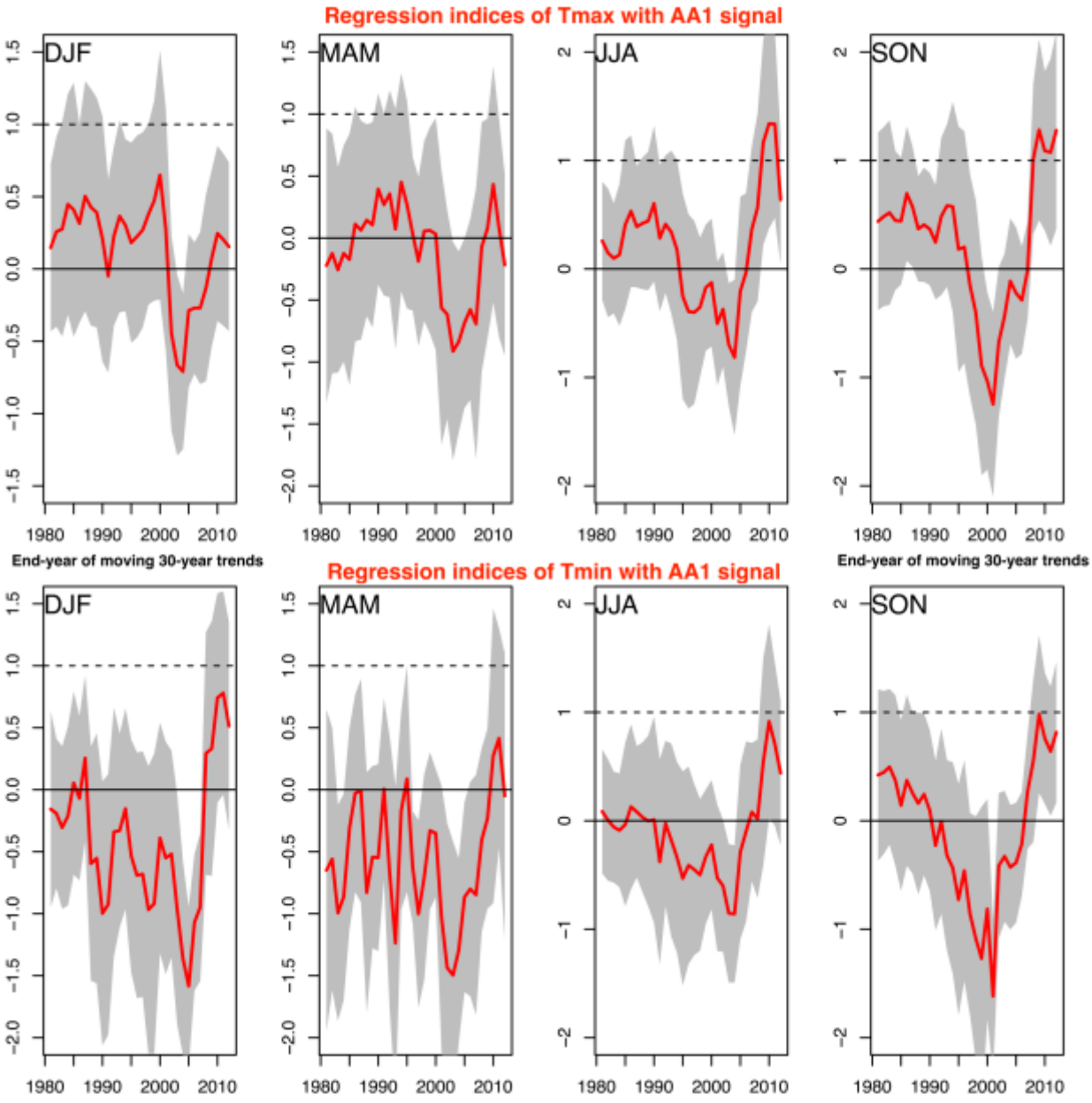

Figure 9: First (second) row seasonal regression indices of observed moving 30-year trend pattern of Tmax (Tmin), over the period 1952–2012, onto the AA1 response pattern. *The vertical axes* denote the regression indices. *The horizontal axes* show the end-year of moving 30-year trends. The grey shaded area indicates the 97.5th %tile range of regression indices in a stationary climate derived from 600 non-overlapping control run segments. *The dotted lines* mark regression indices equal to unity, and *the solid lines* mark regression indices equal to zero. Detection of an anthropogenic aerosol signal can be claimed in those cases where the gray shaded area in Fig 8 excludes "0" and consistency with AA1 signal pattern is claimed in cases where the gray shaded area does not include "0" but includes "1".

Acknowledgments: We acknowledge the support provided by the US National Science Foundation AGS-1547899. We further acknowledge the Cluster of Excellence 'CliSAP' (EXC177), Universität Hamburg, funded through the German Science Foundation (DFG). Data used in this paper are available from the corresponding author (barkhora@g.ucla.edu) upon request.

References:

Archer-Nicholls S, Lowe1 D, Schultz D.M, and McFiggans G (2016) Aerosol–radiation–cloud interactions in a regional coupled model: the effects of convective parameterization and resolution. Atmos. Chem. Phys., 16, 5573–5594.

Arora, V. K., J. F. Scinocca, G. J. Boer, J. R. Christian, K. L. Denman, G. M. Flato, V. V. Kharin, W. G. Lee, and W. J. Merryfield (2011), Carbon emission limits required to satisfy future representative concentration pathways of greenhouse gases, Geophys. Res. Lett., 38(5), L05805, doi:10.1029/2010GL046270.

Artaxo et al., (2013) Atmospheric aerosols in Amazonia and land use change: from natural biogenic to biomass burning conditions, Faraday Discuss., 165, 203–235, doi: 10.1039/C3FD00052D.

Barkhordarian A, von Storch H, Zorita E and J Gómez-Navarro (2016) An attempt to deconstruct recent climate change over the Baltic Sea basin. Journal of Geophysical Research - Atmosphere, 121, doi:10.1002/2015JD024648.

Barkhordarian A, von Storch H and Zorita E (2012b) Anthropogenic forcing is a plausible explanation for the observed surface specific humidity trends over the Mediterranean area. Geophysical Research Letters, 39, L19706, doi:10.1029/2012 GL053026.

Barkhordarian, A., J. Bhend, and H. von Storch (2012a), Consistency of observed near surface temperature trends with climate change projections over the Mediterranean region, Clim. Dyn., 38, 1695–1702.

Barkhordarian, A., H. von Storch, and J. Bhend (2013), The expectation of future precipitation change over the Mediterranean region is different from what we observe, Clim. Dyn., doi:10.1007/s00382-012-1497-7.

Bhend, J., and H. von Storch (2008), Consistency of observed winter precipitation trends in northern Europe with regional climate change projections. Climate Dynamics, 31, 17-28.

Blázquez J, Nestor-Nuñez M and S Kusunoki (2012) Climate Projections and Uncertainties over South America from MRI/JMA Global Model Experiments. Atmospheric and Climate Sciences, 2012, 2, 381-400.

Bradley, R. S., F. T. Keimig, H. F. Diaz, and D. R. Hardy (2009) Recent changes in freezing level heights in the Tropics with implications for the deglacierization of high mountain regions. Geophysical Research Letters, 36, L17701, doi:10.1029/2009GL037712.

Braganza, K., D. J. Karoly, and J. M. Arblaster (2004), Diurnal temperature range as an index of global climate change during the twentieth century, Geophys. Res. Lett., 31, L13217, doi:10.1029/2004GL019998.

Chadwick R, Good P, Martin g and D P Rowell (2016) Large rainfall changes consistently projected over substantial areas of tropical land. Nature Climate Change 6,177–181. doi:10.1038/nclimate2805

Cox et al (2000) Acceleration of global warming due to carbon-cycle feedbacks in a coupled climate model. Nature 408, 184-187 (9 November 2000) | doi:10.1038/35041539.

de Barros Soares, D., Lee, H., Loikith, P. C., Barkhordarian, A. and Mechoso, C. R. (2017), Can significant trends be detected in surface air temperature and precipitation over South America in recent decades?. Int. J. Climatol., 37: 1483–1493. doi:10.1002/joc.4792

Easterling, D.R., and T.C. Peterson (1995), A new method for detecting undocumented discontinuities in climatological time-series. Int. J. Clim. 15:369-377.

Exbrayat JF, Williams M. 2015. Quantifying the net contribution of the historical Amazonian deforestation to climate change. Geophys. Res. Lett. 42: 2968–2976, doi: 10.1002/2015gl063497.

Falvey, M., and R. D. Garreaud (2009), Regional cooling in a warming world: Recent temperature trends in the southeast Pacific and along the west coast of subtropical South America (1979–2006), J. Geophys. Res., 114, D04102, doi:10.1029/2008JD010519

Gillett, N. P., V. K. Arora, G. M. Flato, J. F. Scinocca, and K. von Salzen (2012), Improved constraints on 21st-century warming derived using 160 years of temperature observations, Geophys. Res. Lett., 39(1), L01704, doi:10.1029/2011GL050226.

Grau, H. R., and M. Aide. 2008. Globalization and land-use transitions in Latin America. *Ecology and Society* **13**(2): 16.

Guyon, P., et al. (2003), Physical properties and concentration of aerosol particles over the Amazon tropical forest during background and biomass burning conditions, Atmos. Chem. Phys., 3, 951– 967.

Harris, I., Jones, P.D., Osborn, T.J., and D.H. Lister (2014), Updated high-resolution grids of monthly climatic observations – the CRU TS3.10 Dataset. Int. J. Climatology, 34, 623-642, Doi: 10.1002/joc.3711

Hodnebrog, Ø. et al. (2014) How shorter black carbon lifetime alters its climate effect. Nat. Commun. 5:5065 doi: 10.1038/ncomms6065.

IPCC. 2013. Climate Change 2013: The Physical Science Basis. Contribution of Working Group I to the Fifth Assessment Report of the Intergovernmental Panel on Climate Change. Cambridge University Press: Cambridge, UK and New York, NY, 1535 pp.

Jiménez-Muñoz, J. C., J. A. Sobrino, C. Mattar, and Y. Malhi (2013), Spatial and temporal patterns of the recent warming of the Amazon forest, J. Geophys. Res. Atmos., 118, 5204–5215, doi:10.1002/jgrd.50456.

Jones, G. S., Christidis, N., and Stott, P. A (2011) Detecting the influence of fossil fuel and bio-fuel black carbon aerosols on near surface temperature changes, Atmos. Chem. Phys., 11, 799-816, doi:10.5194/acp-11-799-2011.

Jones, P.W. (1999), First- and second-order conservative remapping schemes for grids in spherical coordinates. Mon. Wea. Rev., 127:2204-2210.

Kirkev.g, A., et al. (2013), Aerosol-climate interactions in the Norwegian Earth System Model—NorESM1-M, Geosci. Model Dev., 6(1), 207–244, doi:10.5194/gmd-6-207-2013.

Knutson, T. R., F. Zeng, and A. T. Wittenberg, 2013: Multimodel assessment of regional surface temperature trends: CMIP3 and CMIP5 twentieth-century simulations. J. Climate,26, 8709–8743, doi:10.1175/JCLI-D-12-00567.1

Kumar, S., R. P. Allan, F. Zwiers, D.M. Lawrence, and P. A. Dirmeyer (2015), Revisiting trends in wetness and dryness in the presence of internal climate variability and water limitations over land, Geophys. Res. Lett., 42, 10,867–10,875, doi:10.1002/2015GL066858.

Forster, P., et al. (2007), Changes in atmospheric constituents and in radiative forcing, in Climate Change 2007: The Physical Science Basis. Contribution to Working Group I to the Fourth Assessment Report of the Intergovernmental Panel on Climate Change, edited by S. Solomon et al., pp. 129–234, Cambridge Univ. Press, Cambridge, United Kingdom and New York, NY, USA.

Lin, J. C., T. Matsui, R. A. Pielke Sr., and C. Kummerow (2006), Effects of biomass-burning-derived aerosols on precipitation and clouds in the Amazon Basin: a satellite-based empirical study, J. Geophys. Res., 111, D19204, doi:10.1029/2005JD006884.

Lohmann, U., and J. Feichter (2005), Global indirect aerosol effects: A review, Atmos. Chem. Phys., 5, 715–737.

Loikith P. C., Detzer J., Mechoso C. R., Lee K. & Barkhordarian A. *(*2017*)*. The Influence of Recurrent Modes of Climate Variability on the Occurrence of Monthly Temperature Extremes over South America. Journal of Geophysical Research: Atmospheres, 122. https://doi.org/10.1002/2017JD027561.

Marengo, J. A., 1992: Interannual variability of surface climate in the Amazon basin. *Journal of Climatology*, DOI: 10.1002/joc.3370120808.

Marengo, J.A., Chou, S.C., Kay, G. et al. (2012) Development of Regional Future Climate Change Scenarios in South America Using the Eta CPTEC/HadCM3 Climate Change Projections: Climatology and Regional Analyses for the Amazon, São Francisco and the Paraná River Basins. Clim Dyn (2012) 38: 1829. https://doi.org/10.1007/s00382-011-1155-5.

Mariano G.L, Mariano E.V.C and A.m. de Oliveira (2014) Aerosol Optical Depth over South America: The Influence of Biomass Burning. *Air Pollution and Pollutants*. Editor by: Hejing Wang. *AcademyPublish.org.* ISBN: 978-1-941249-02-4. pp:74-89.

Martin, S. T., et al. (2010), Sources and properties of Amazonian aerosol particles, Rev. Geophys.,48, RG2002, doi:10.1029/2008RG000280.

Mantua, N. J., and S. R. Hare, 2002: The Pacific Decadal Oscillation. *Journal of Oceanography*, **58**, 35-44.

Meehl, G. A., et al. (2013), Climate change projections in CESM1(CAM5) compared to CCSM4, J. Clim., 26(17), 6287–6308, doi:10.1175/JCLI-D-12-00572.1.

Meinshausen, M., S. J. Smith, K. V. Calvin, J. S. Daniel, M. L. T. Kainuma, J.-F. Lamarque, K. Matsumoto, S. A. Montzka, S. C. B. Raper, K. Riahi, A. M. Thomson, G. J. M. Velders and D. van Vuuren (2011). "The RCP Greenhouse Gas Concentrations and their Extension from 1765 to 2300." Climatic Change (Special Issue), DOI: 10.1007/s10584-011-0156-z

Nuñez, M. N, Solman, S.A. and M. F. Cabré (2009) "Regional Climate Change Experiments over Southern South America. II: Climate Change Scenarios in the Late Twenty- First Century," *Climate Dynamics*, Vol. 32, No. 7-8, pp. 1081-1095. doi:10.1007/s00382-008-0449-8.

Posselt, R., Mueller, R., Stockli, R. and J. Trentmann (2011), Spatial and Temporal Homogeneity of Solar Surface Irradiance across Satellite Generations. Remote Sens., 3, 1029-1046; doi: 10.3390/rs3051029.

Procopio, A. S., P. Artaxo, Y. J. Kaufman, L. A. Remer, J. S. Schafer, and B. N. Holben (2004), Multiyear analysis of Amazonian biomass burning smoke radiative forcing of climate, Geophys. Res. Lett., 31, L03108, doi:10.1029/2003GL018646.

Ramanathan, V., et al. (2001), Aerosols, climate, and the hydrological cycle, Science, 294, 2119–2124.

Rosário, N. E., Longo, K. M., Freitas, S. R., Yamasoe, M. A., and Fonseca, R. M. (2013) Modeling the South American regional smoke plume: aerosol optical depth variability and surface shortwave flux perturbation, Atmos. Chem. Phys., 13, 2923-2938, https://doi.org/10.5194/acp-13-2923-2013.

Rotstayn, L. D., S. J. Jeffrey, M. A. Collier, S. M. Dravitzki, A. C. Hirst, J. I. Syktus, and K. K. Wong (2012), Aerosol- and greenhouse gas-induced changes in summer rainfall and circulation in the Australasian region: A study using single-forcing climate simulations, Atmos. Chem. Phys., 12(14), 6377–6404, doi:10.5194/acp-12-6377-2012.

Sánchez E et al (2015) Regional climate modelling in CLARIS-LPB: a concerted approach towards twenty first century projections of regional temperature and precipitation over South America. Climate Dynamics. DOI 10.1007/s00382-014-2466-0

Schulz, N., J. P. Bosier, and P. Aceituno (2012), Climate change along the arid coast of northern Chile, Int. J. Climatol., 32(12), 1803–1814.

Thompson, D. W. J. and J. M. Wallace (2000) Annular Modes in the Extratropical Circulation. Part I: Month-to-Month Variability. *J. Climate*, **13**, 1000-1016.

Urrutia, R., *and* M. Vuille *(*2009*),* Climate change projections for the tropical Andes using a regional climate model: Temperature and precipitation simulations for the end of the 21st century, J. Geophys. Res., 114, D02108, *doi:*10.1029/2008JD011021

van der Werf, G. R., Randerson, J. T., Giglio, L., Collatz, G. J., Mu, M., Kasibhatla, P. S., Morton, D. C., DeFries, R. S., Jin, Y., and van Leeuwen, T. T. (2010) Global fire emissions and the contribution of deforestation, savanna, forest, agricultural, and peat fires (1997– 2009), Atmos. Chem. Phys., 10, 11707–11735, doi:10.5194/acp- 10-11707-2010.

Vose, R. S., D. R. Easterling, and B. Gleason (2005), Maximum and minimum temperature trends for the globe: An update through 2004, Geophys. Res. Lett., 32, L23822, doi:10.1029/2005GL024379.

Vuille, M., E. Franquist, R. Garreaud, W. S. Lavado Casimiro, and B. Cáceres (2015), Impact of the global warming hiatus on Andean temperature, J. Geophys. Res. Atmos., 120, 3745–3757, doi:10.1002/ 2015JD023126.

Wilcox, L. J., E. J. Highwood, and N. J. Dunstone (2013), The influence of anthropogenic aerosol on multi-decadal variations of historical global climate, Environ. Res. Lett., 8(2), 024,033, doi:10.1088/1748-9326/8/2/024033.